

# Thermal stability and decomposition kinetics of $\text{Li}_2\text{Al}_4\text{CO}_3(\text{OH})_{12} \cdot 3\text{H}_2\text{O}$

C. A. DREWIEN, D. R. TALLANT, M. O. EATOUGH

*Materials and Process Sciences Centre, Sandia National Laboratories, Albuquerque, NM 87185 USA*

The thermal stability of lithium containing hydrotalcite, a material that has potential application for providing atmospheric corrosion protection to aluminium alloys, was investigated. Lithium aluminium carbonate hydroxide hydrate ( $\text{Li}_2\text{Al}_4\text{CO}_3(\text{OH})_{12} \cdot 3\text{H}_2\text{O}$ ) coatings were prepared by immersion of an 1100 aluminium alloy into a lithium carbonate–lithium hydroxide solution, and the bulk material was prepared by precipitation in the same solution. Thermal stability of the coatings and the bulk material existed to around 150 °C. Above this temperature, interlayer water was expelled, followed by loss of structural water and carbon dioxide. The kinetic parameters for interlayer water loss have been determined, and water loss can be described by a Johnson–Mehl–Avrami rate equation.

## 1. Introduction

Traditional surface finishing technologies for enhancing corrosion resistance of aluminium and its alloys include de-oxidizing, plating, priming, conversion coating, and painting, processes which may contain hexavalent chromium as an active bath agent or pigment. Hexavalent chromium, a known human carcinogen, is being regulated under federal legislation including the Clean Air Act, Clean Water Act, Pollution Prevention Act, Resource Conservation and Recovery Act (RCRA), Comprehensive Environmental Response, Compensation, and Liability Act (CERCLA), and others. Traditional surface finishing technologies will therefore be performed under strictly controlled conditions and with much added cost. For these reasons, efforts to identify, develop, and implement simple and cost effective methods for achieving desirable surface properties utilizing environmentally safe chemicals are underway.

One possible replacement for chromate conversion coatings is based upon the novel use of lithium aluminium carbonate hydroxide hydrate (hydrotalcite) as a corrosion resistant coating for aluminium alloys [1]. Hydrotalcite coatings impart corrosion resistance to the underlying Al substrate, and processing of the coatings, like chromate conversion coatings, is performed by simple immersion of the substrate into an aqueous solution [1]. These features make the lithium aluminium carbonate hydroxide hydrate coating, hereafter referred to as a hydrotalcite coating, a very attractive and environmentally safe candidate for replacement of chromate conversion coatings on aluminium alloys. The processing, microstructure, composition, and desired properties of hydrotalcite coatings have been discussed elsewhere [2].

Because the coatings may be exposed to elevated temperatures during use and/or paint layers may be applied to the coating, decomposition of the coating could lead to inadequate corrosion properties and/or off-gassing from the coating could cause blistering of the paint. In fact, it was reported that the corrosion behaviour of these coatings deteriorates after heat treatments at temperature above 250 °C [2]. Thus, it is the purpose of this investigation to determine the thermal stability of lithium aluminium carbonate hydroxide hydrate, the decomposition process of the material, and the decomposition kinetics for decomposition reactions in which gas is evolved.

## 2. Experimental procedure

### 2.1. Coating processing

The coating of many aluminium alloys with hydrotalcite is possible; in this study, only Al 1100, or commercially pure aluminium was used. The 3.2 mm thick sheet stock material was obtained in 102 mm × 127 mm sections. Samples were cleaned by abrading the surfaces in a dilute solution of Alconox or by vapour degreasing with trichloroethane. An immersion in 65 °C sodium silicate–sodium carbonate solution removed organic and inorganic debris from the sample surfaces, and then samples were rinsed and de-oxidized in a room temperature nitric acid-1 M ammonium bifluoride bath. Samples were rinsed in de-ionized water and coated using a 15 min immersion in a room temperature bath of 0.1 M lithium carbonate solution whose pH was 11.15 or  $12.05 \pm 0.5$  (0.3 M lithium hydroxide addition).

## 2.2. Powder processing

Hydrotalcite powder was formed by precipitation from an aluminium saturated solution of 0.1 M lithium carbonate. Aluminium was introduced by either the addition of the above mentioned panels or sodium aluminate. The precipitate was filtered from solution, rinsed and filtered, and dried at room temperature.

## 2.3. Compositional analysis

The Al and Li contents of the precipitate were analysed by ICP-AES (atomic emission spectroscopy) using an ARL 3580. The aluminium to lithium ratio was  $1.8 \pm 0.12$ .

## 2.4. Crystallographic analysis

Phase identification and crystal structure determinations were investigated using grazing incidence X-ray diffraction analysis (GIXRD). GIXRD utilizes a parafocusing geometry where the incident angle is maintained at an angle which is generally less than about  $2^\circ$  and the detector is scanned through all angles of  $2\theta$ . GIXRD is useful for limiting the effective penetration of X-rays to depths of a few tens to a few hundred nanometres [3].

For our experiments, we used a Siemens D500 powder diffractometer equipped with a thin film attachment consisting of a long set of soller slits on the receiving side. To attain maximum resolution we used  $0.1^\circ$  scatter slits, a diffracted beam monochromator consisting of a flat (100) cut lithium fluoride crystal, and a scintillation counter. The radiation used was copper ( $k_\alpha$ ). To limit effective penetration to about 100 nm we used a grazing angle of  $0.2^\circ$  on coated samples.

## 2.5. Structural analysis

Argon ion laser Raman spectroscopy was performed using an excitation wavelength of 514 nm from an argon ion laser and using a triple spectrograph with a charge-coupled detector and a microscope attachment.

## 2.6. Thermal stability determination

Thermal stability of the powder was analysed using P1 Thermal Sciences Thermo-gravimetric analyser followed by a Biorad 40 Fourier transform infrared spectrometer (TGA-FTIR). A heating rate of  $15^\circ\text{C}$  per min was employed, and the water and carbon dioxide content of the precipitate was determined by mass change. A Perkin-Elmer DSC-7 was used to monitor reaction temperatures and establish kinetics of dehydration through the Lee-Kim model [4].

Both the powder and coatings were heated for 1–3 h in a box furnace at temperatures between  $70$ – $300^\circ\text{C}$ , and the powder was heated at  $400$ ,  $550$ ,  $650$ , and  $800^\circ\text{C}$  for 1 h. The samples were then analysed for decomposition products using X-ray diffraction (XRD) and Raman spectroscopy techniques.

## 3. Results

### 3.1. Thermal stability

The results of the TGA-FTIR analyses showed the loss of water and carbon dioxide during the heating of hydrotalcite powder to temperatures of  $800^\circ\text{C}$ . The thermal profile is shown in Fig. 1. Endothermic peaks exist at  $177$ ,  $275$ ,  $532$ , and  $632^\circ\text{C}$ . Table I shows the weight loss of the samples and the species emitted from the samples. Water loss was approximately 13% at temperatures near  $177^\circ\text{C}$ ; and total weight loss due to release of carbon dioxide and water from the structure was 35% at  $632^\circ\text{C}$ .

In order to determine changes in the material due to each endothermic reaction, powder was heated for one or more hours in air at temperatures of  $200$ ,  $300$ ,  $400$ ,  $550$ ,  $650$ , and  $800^\circ\text{C}$ . The samples were then analysed using XRD and Raman spectroscopy techniques in order to determine the decomposition products. The resulting XRD and Raman spectra are provided in Figs. 2 and 3, respectively.

The powder heated to  $200^\circ\text{C}$  for 1 h consisted of hydrotalcite, however both the Raman spectra and the TGA-FTIR data indicated water loss had occurred. The remaining material was approximately  $\text{Li}_2\text{Al}_4\text{CO}_3(\text{OH})_{12}$  without interlayer water. Heating to  $300^\circ\text{C}$  and  $400^\circ\text{C}$  brought about the formation of a carbonate peak at  $1090\text{ cm}^{-1}$  in the Raman spectra, and an XRD pattern consistent with  $\text{Li}_2\text{Al}_4\text{O}_7(\text{CO}_2)_{0.1}\cdot 10.5\text{H}_2\text{O}$  was obtained. The presence of waters of hydration in the lithium aluminium oxide carbonate specie was not suggested by Raman data. Thus, it is suggested although not confirmed that the specie was  $\text{Li}_2\text{Al}_4\text{O}_7(\text{CO}_2)_{0.1}$ ; however, it is acknowledged that no effort to prevent adsorption of water after heat treatment was

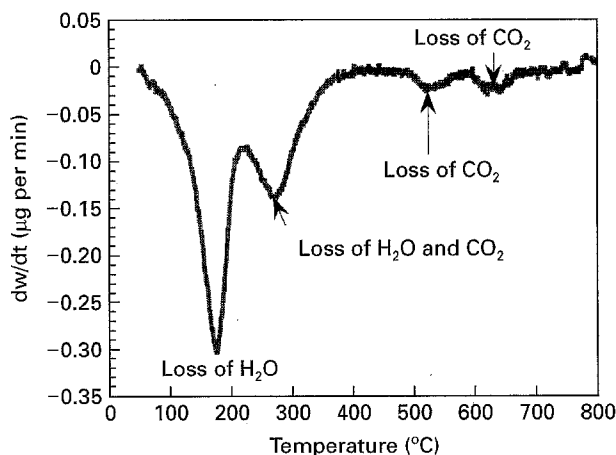


Figure 1 TGA-FTIR derivative plot showing decomposition of hydrotalcite at  $177$ ,  $275$ ,  $532$ , and  $632^\circ\text{C}$  by loss of water and carbon dioxide.

TABLE I TGA-FTIR results

Temperature ( $^\circ\text{C}$ )	Species	Weight loss (%)
177	$\text{H}_2\text{O}$	13
275	$\text{H}_2\text{O}$ , $\text{CO}_2$	26
532	$\text{CO}_2$	34
632	$\text{CO}_2$	35

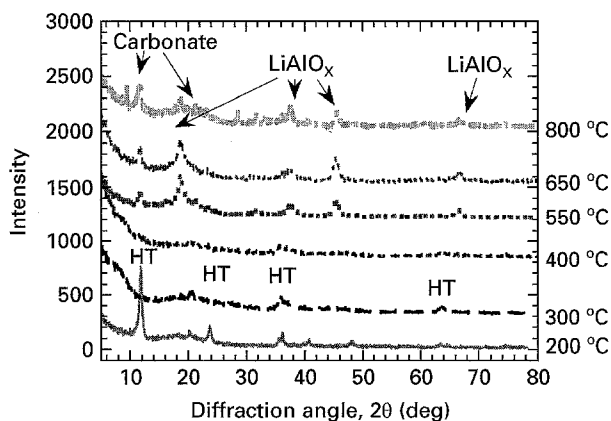


Figure 2 X-ray diffraction profiles for powder versus heat treatment temperature.

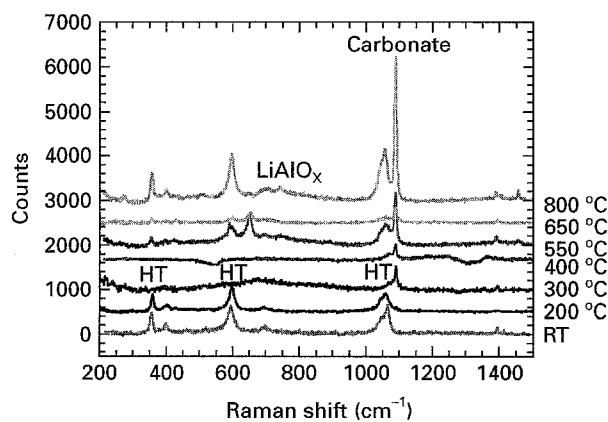


Figure 3 Raman spectra for powder versus heat treatment temperature.

made. Additionally,  $\text{LiAlO}_2$  was detected in the Raman and XRD patterns. The powder contained  $\alpha\text{-LiAlO}_2$ ,  $\gamma\text{-Al}_2\text{O}_3$ , and  $\text{Li}_2\text{Al}_4\text{O}_7(\text{CO}_2)_{0.1}$  after heating to 550 and 650 °C. A lithium aluminium oxide phase is indicated by the peak in the Raman spectra at  $653\text{ cm}^{-1}$ , and the XRD pattern supports the presence of  $\text{LiAlO}_2$ . A broad hydroxyl band exists in the Raman spectra for the sample heated to 650 °C. Note that the Raman spectra of the sample at 550 °C and 650 °C are nearly identical except for the intensities of the peaks. Due to the nature of sampling, lower intensities were obtained from the 650 °C sample than the 550 °C sample, but the spectra are virtually identical. After heating to 800 °C, the powder contained  $\alpha\text{-LiAlO}_2$ ,  $\gamma\text{-LiAlO}_2$ ,  $\text{LiAl}_5\text{O}_8$ ,  $\gamma\text{-Al}_2\text{O}_3$ , and  $\text{Li}_2\text{Al}_4\text{O}_7(\text{CO}_2)_{0.1}$ . The Raman bands in the spectra at 800 °C suggest a structure similar to hydroxalcite; the material may have re-absorbed carbon dioxide and water to yield the broad peaks in the vicinity of the hydroxalcite peaks. Also, the strong carbonate band at  $1088\text{ cm}^{-1}$  suggests more carbonate than the  $\text{Li}_2\text{Al}_4\text{O}_7(\text{CO}_2)_{0.1}$  composition. XRD peaks with  $d$ -spacings of 0.94 nm and 0.312 nm may be attributed to lithium aluminium hydride or an isomorphous phase of lithium aluminium manganese oxide hydroxide.

The thermal stability of hydroxalcite is maintained to temperatures at which interlayer water is removed, approximately 175 °C. With loss of interlayer water,

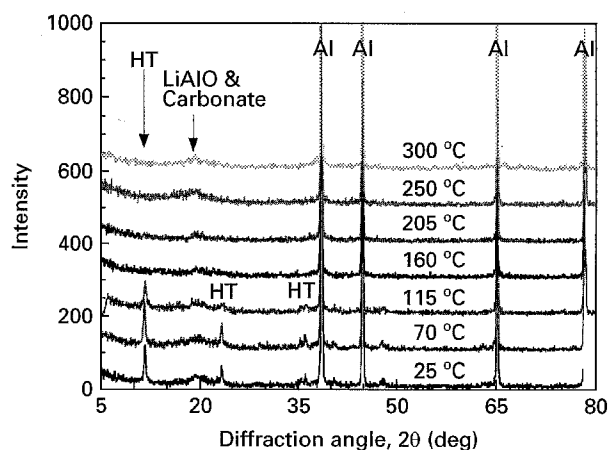


Figure 4 X-ray diffraction patterns from hydroxalcite coatings heated for 3 h at the temperatures indicated show evolution of  $\text{LiAlO}_2$  and  $\text{Li}_2\text{Al}_4\text{O}_7(\text{CO}_2)_{0.1}$  in the coating.

the hydroxalcite structure is maintained. The change in weight being 13% corroborates the removal of 3 molecules of water from the original formula of hydroxalcite, resulting in  $\text{Li}_2\text{Al}_4\text{CO}_3(\text{OH})_{12}$ . The second peak observed in the TGA profile corresponded to the loss of water and some carbon dioxide. The change in weight was again 13% suggesting that more water molecules are removed. Further water loss after removal of the interlayer water could only occur if structural water bound to the aluminium in the cation or brucite layers results. The loss of bound water from the positively-charged brucite layers was also reported by Miyata [5] for the decomposition of synthetically prepared hydroxalcite containing magnesium and aluminium. With loss of structural water and some carbon dioxide, the sample converts towards  $\text{LiAlO}_2$  and  $\text{Li}_2\text{Al}_4\text{O}_7(\text{CO}_2)_{0.1}$  near 275 °C. With continued heating to temperatures above 500 °C,  $\gamma\text{-Al}_2\text{O}_3$  is detected and finally the original hydroxalcite powder transforms towards  $\gamma$ -alumina and lithium aluminate ( $\text{LiAl}_5\text{O}_8$ ) above 632 °C. The final peaks resulted from outgassing of carbon dioxide only. The change in weight for the loss of 6 molecules of water and one molecule of carbon dioxide is calculated at 34.56 w/o; the experimentally determined value was  $35 \pm 0.25$  w/o. The sequence of decomposition events is consistent with reports on thermal decomposition of lithium aluminium phosphate hydroxide hydrate and lithium aluminium borate hydroxide hydrate [6, 7]. However, the interpretation of the thermal stability of hydroxalcite was reported by reference [8] to extend to 275 °C as the amount of carbon dioxide in the structure increased.

Coatings heated at 70, 115, 160, 205, and 300 °C for 3 h were analysed using X-ray diffraction. The results, illustrated in Fig. 4, showed a similar sequence of hydroxalcite decomposition in that hydroxalcite decomposed to an amorphous or finely crystalline phase and finally towards  $\text{LiAlO}_2$  and  $\text{Li}_2\text{Al}_4\text{O}_7(\text{CO}_2)_{0.1}$ .

The kinetics of interlayer water loss were determined from differential scanning calorimetry (DSC) data and the utilization of the Lee-Kim kinetics model [4]. Small samples of hydroxalcite powder, heated at rates between 5 and 50 °C per min from

TABLE II Peak temperature versus heating rate determined from DSC for precipitate powder

Heating Rate (°C per min)	Temperature (°C) Peak 1	Temperature (°C) Peak 2	Temperature (°C) Peak 3
5	117.2	155.0	264.2
10	123.9	170.0	255.3
15	132.0	180.0	270.4
20	132.5	182.8	272.8
50	145.1	198.5	283.9

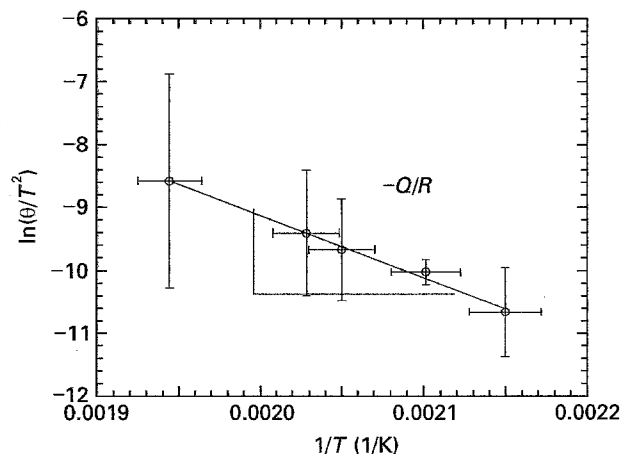


Figure 5 Kissinger plot of DSC data for endothermic reaction associated with loss of interlayer water.

room temperature to 350 °C, yielded three endothermic peaks: i) in the vicinity of 120 °C ( $\sim 1.6 \text{ J g}^{-1}$ ) ii) in the vicinity of 175 °C ( $\sim 325 \text{ J g}^{-1}$ ) and iii) in the vicinity of 275 °C ( $\sim 60 \text{ J g}^{-1}$ ). An increase in the peak temperature for the removal of water in hydrotalcite was observed within an increase in heating rate  $\theta$  during heating in DSC. The peak temperature versus heating rate data are provided in Table II.

The data for the second endothermic peak in the DSC profile, corresponding to the loss of interlayer water, is plotted in Fig. 5 in the form of a Kissinger plot. A Kissinger plot relates the inverse of the peak temperature of transformation ( $T$ ) to the heating rate divided by the peak temperature of transformation squared e.g.,  $(\theta/T^2)$ . The slope of the line is equal to  $-Q/R$  where  $Q$  is the activation energy for the transformation and  $R$  is the gas constant. An activation energy value of  $829 \pm 5\%$  kJ per mole was found for the reaction at 175 °C.

The  $Q$  value was then used in the Lee–Kim kinetics model for non-isothermal data in order to determine the kinetics parameters— $n$ , the time exponent;  $c$ , the impingement factor; and  $k_0$ , the pre-exponential factor where  $k = k_0 \exp(-Q/RT)$ . A Lee–Kim plot of  $\ln(p(z))$  versus  $G(c)$  was developed for  $c$  equal to values of 0 or 1; a thorough explanation of the terms  $\ln(p(z))$  and  $G(c)$  can be found in reference [4]. Fig. 6 (a and b) show the Lee–Kim plots for the reaction when heating rates of 5 and 10 °C per min were used;  $c = 0$  provided the best fit of the data to straight lines. The slopes of the lines, which are equal to  $n$ , have values of approximately 1.9, and the intercepts of the lines, which are

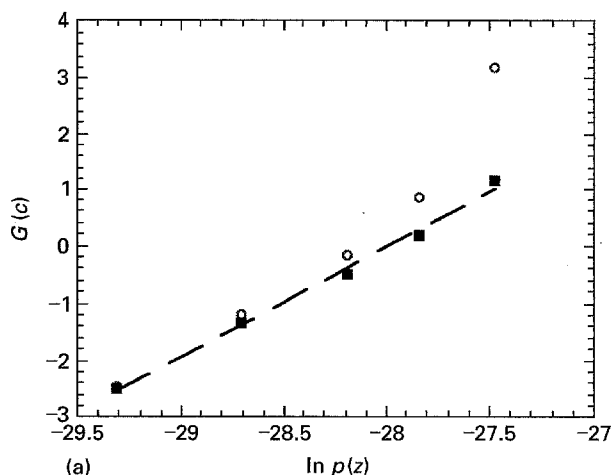


Figure 6a Lee–Kim plot for endothermic reaction of interlayer water loss using data from heating at a rate of 5 °C per min. Data shown for the conditions; (■)  $G(c = 0)$  and (○)  $G(c = 1)$ .

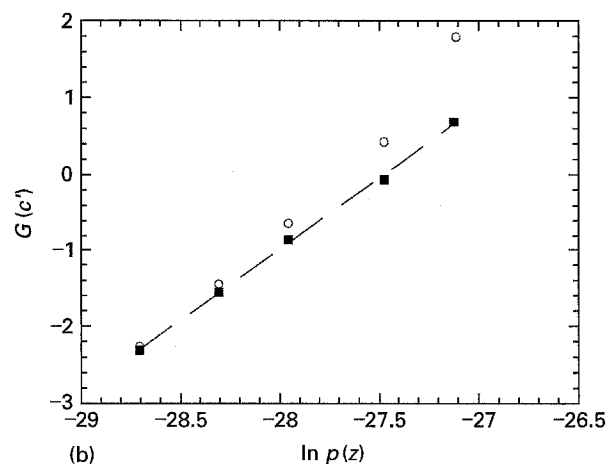


Figure 6b Lee–Kim plot for endothermic reaction of interlayer water loss using data from heating at a rate of 10 °C per min. Data shown for the conditions; (■)  $G(c = 0)$  and (○)  $G(c = 1)$ .

equal to  $n \ln(k_0 Q/RT)$ , have values of about 52, such that the value for  $\ln k_0$  is about 20.4 when the time unit was chosen as minutes.

For  $c = 0$ , the Lee–Kim model allows the use of the Johnson–Mehl–Avrami kinetics equation to describe reaction kinetics of the transformation; in this instance to describe removal of interlayer water from the hydrotalcite. The fraction of interlayer water driven off ( $y$ ) during a given heat treatment can be approximated through use of the following equation:

$$y = 1 - \exp(-(kt)^n)$$

when  $n = 1.9$  and  $k = 7.23 \times 10^8 \exp(-9980/T)$  if the temperature ( $T$ ) is in units of K and time ( $t$ ) is in minutes. Here the significance of  $n$  is unclear. The value  $Q$  obtained for the activation energy would relate to the bonding of interlayer water molecules within the hydrotalcite. As is shown in Fig. 7, which illustrates the fraction of interlayer water loss versus temperature of heating at times of 30, 60, 90, and 120 min, the loss of interlayer water for a half hour heat treatment at 100 °C is minimal.

Much more scatter exists in the data for the third endothermic peak, which might be expected because

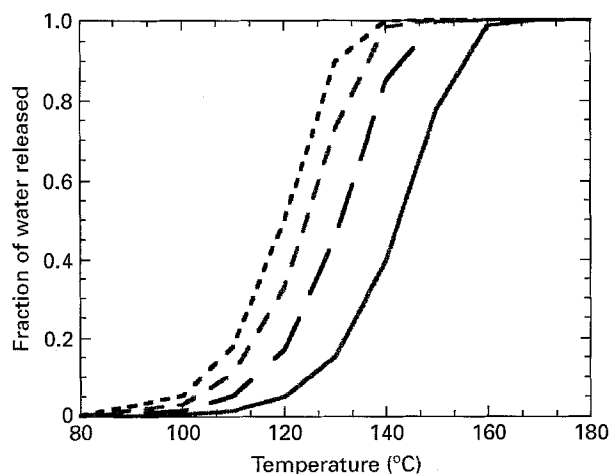


Figure 7 Percentage of interlayer water loss in hydrotalcite versus temperature for heat treatment at (—) 30 min, (---) 60 min, (- -) 90 min and (- · -) 120 min.

the loss of both water and carbon dioxide may not be occurring at the same rate. As such, no attempt was made to model the kinetics reaction for this transformation.

#### 4. Summary and conclusions

Thermal stability of lithium containing hydrotalcite is maintained to temperatures near 175 °C at which point the material undergoes a 13% weight change corresponding to loss of three molecules of interlayer water. The resulting material is approximately  $\text{Li}_2\text{Al}_4\text{CO}_3(\text{OH})_{12}$ . At temperatures near 275 °C more water loss and carbon dioxide loss occur, resulting in a subsequent 13% weight loss for the material. The transformation towards  $\text{Li}_2\text{Al}_4\text{O}_7(\text{CO}_2)_{0.1}$  and  $\text{LiAlO}_2$  results. Heating above 532 °C yields more weight loss by carbon dioxide as the material transforms to  $\text{Al}_2\text{O}_3$  and  $\text{LiAlO}_2$ . Finally, at temperatures greater than 632 °C, the material decomposes towards  $\text{LiAl}_5\text{O}_8$  and  $\text{Al}_2\text{O}_3$ .

The kinetics of interlayer water loss were determined using non-isothermal conditions and applying a transformation kinetics model developed by Lee and Kim [4]. An activation energy of 82.9 kJ per mole was obtained for the loss of interlayer water. The kinetic

equation describing interlayer water loss is

$$y = 1 - \exp \left[ - \left\{ \left( 7.23 \times 10^8 \times \exp \left( - \frac{9980}{T} \right) \right) \times t \right\}^{1.9} \right]$$

These results suggest that heat treatment to 100 °C for 30 min should not adversely affect the composition of the coating by water loss. Additionally, the previous observations regarding deterioration of corrosion protection of the coating to the underlying aluminium substrate for heat treatments at temperatures greater than 250 °C can be attributed to the decomposition of hydrotalcite towards  $\text{LiAlO}_2$  and  $\text{Li}_2\text{Al}_4\text{O}_7(\text{CO}_2)_{0.1}$  in the vicinity of 250 °C. Thus, if desired, water may be driven off of the coating by heating prior to any surface treatment, such as primer or paint applications, without adversely affecting the corrosion protection afforded by the conversion coating.

#### Acknowledgements

The authors appreciate the help from R. Buchheit, J. Bullen, M. Gonzales, K. Alam, M. Bode, R. Garcia, and D. Goel. This work was performed at Sandia National Laboratories, operated for the Department of Energy under contract number DE-AC04-94A185000.

#### References

1. R. G. BUCHHEIT, M. BODE and G. E. STONER, *Corrosion* **50** (1994) 205.
2. R. G. BUCHHEIT, C. A. DREWIEN, M. A. MARTINEZ and G. E. STONER, Corrosion '95 conference, paper 390, Orlando, FL, National Association of Corrosion Engineers (1995).
3. R. P. GOEHNER and M. O. EATOUGH, *Powder Diffraction* **7** (1992) 2.
4. E. LEE and Y. G. KIM, *Acta Metall. Mater.* **38** (1990) 1677.
5. S. MIYATA, *Clay and Clay Minerals* **23** (1975) 369.
6. V. P. DANILOV, I. N. LEPESHKOV, Y. Y. KHARITONOV, T. O. ASHCYAN, L. V. GOEVA and O. F. KOSTYLEVA, *Russian J. of Inorg. Chem.* **22** (1977) 1137.
7. A. R. POEPELMEIER and S.-J. HWU, *Inorg. Chem.* **26** (1987) 3297.
8. E. T. DEVYATKINA, N. P. KOTSUPALO, N. P. TOMILOV and A. S. BERGER, *Russian J. of Inorg. Chem.* **28** (1983) 801.

Received 25th May 1995

and accepted 18th March 1996